Investigation of the Excited State Structure of DCM via Ultrafast Electronic Pump/Vibrational Probe†

Aaron J. Van Tassle, Matthew A. Prantil, and Graham R. Fleming*

Department of Chemistry, University of California, Berkeley, and Physical Biosciences Division, Lawrence Berkeley National Laboratory, Berkeley, California 94720

Received: January 18, 2006; In Final Form: May 16, 2006

Time resolved visible pump, infrared probe transient absorption measurements of the solutes 4-dicyanomethylene-2-methyl-6-(*p*-(dimethylamino)styryl)-4*H*-pyran (DCM) and its isotopomer DCM-d_6 are employed to probe the dynamics of charge transfer state formation in dimethyl sulfoxide (DMSO) and acetonitrile (MeCN). We observe a two stage charge transfer (CT): the first step is an instrument-response-limited charge separation to the dicyanomethylene group, and the second involves a structural evolution of the dimethylamino group. Theoretical calculations and isotopic substitution indicate that the observed vibration is due to the dimethylamino group twisting out of plane, stabilizing the charge separation.

Introduction

The photophysical and photochemical behavior of organic molecules is strongly influenced by charge transfer between electron donating and electron accepting groups following electronic excitation. The way in which the electronic structure evolves is influenced by the solvent and in turn influences the molecular structure and is very difficult to discern from electronic pump−probe or fluorescence spectroscopy. The combination of ultrafast infrared (IR) probing with electronic excitation has the potential to reveal much greater detail about the excited state evolution after initial excitation, and has been used successfully on several systems.[1−7] In this paper, we employ ultrafast electronic excitation and broadband IR probing to study the excited state structural evolution of 4-dicyanomethylene-2-methyl-6-(*p*-(dimethylamino)styryl)-4*H*-pyran (DCM), a laser dye of analogous structure to 4,4′-disubstituted push−pull stilbenes and dimethylaminobenzonitrile (DMABN). DCM has previously been studied, along with several derivatives, for possible use in new graphical displays and organic light emitting diodes.[8−12]

Many of the interesting properties of DCM arise from the charge transfer that occurs in the excited state formed by charge separation between the electron donating dimethylamino group and the electron accepting cyanomethylene groups. Because of the considerable charge separation, the molecule possesses a large, solvent-polarity-dependent Stokes shift and has a drastic change in dipole moment (20.7 D) from the ground state to the excited state.[13−16]

The evolution of DCM from a locally excited electronic state to a charge transfer state has been investigated by numerous authors[13,17−24] who attribute its behavior to one or more of the possible configurational changes which produce the twisted (TICT), conformationally relaxed (CRICT), rehybridized (RICT), and planar (PICT) intramolecular charge transfer states.[4,19,25−33] Previous investigations of DCM[19,23,34] considered the formation of a TICT state involving rotation about the C−N bond linking the dimethylamino group to the aromatic ring, or rotation of the dimethylaminobenzyl moiety, but these experiments lacked any direct probe of structural change. Another proposed state is one analogous to the P* state[26,30,35] of stilbenes in which the molecule adopts a perpendicular conformation about the central double bond as an intermediate between the cis and trans configurations. Electronic structure calculations for DCM using CS INDO (conformation spectra intermediate neglect of differential overlap) have been able to locate a singlet state with a dipole moment large enough to match the experiment, and in this state, DCM adopts a configuration in which the dimethylamino moiety is perpendicular to the aromatic ring.[19]

Recent detailed electronic structure studies of DMABN by Robb and co-workers led to the conclusion that optical excitation initially populates the S_2 state and that radiationless decay via a conical intersection seam can lead to both local and CT states being directly populated, followed by equilibration taking place on the S_1 surface.[36]

The use of IR wavelengths for probing, combined with selective isotopic substitution of DCM, opens up the prospect of determining which functional groups in DCM are involved in the excited state dynamics, thus enabling discrimination between the various possible conformers. By changing the solvent polarity, the role of solvent in the excited state evolution can also be elucidated.

Materials and Methods

Transient absorption experiments were performed with laser pulses from a home-built regenerative amplifier seeded by a Femtosource Compact Pro Ti:Sapphire oscillator (Femtolasers, Inc). This system produces pulses of 35 fs and 400 μJ/pulse at 1 kHz. The pulse was split with 200 μJ being sent into a home-built mid-infrared (mid-IR) optical parametric amplifier (OPA), based on the design of Hamm et al.[37] The design is comprised of a two-pass 800 nm pumped near-IR OPA followed by difference frequency generation. Briefly, a white light continuum seed and two sequential amplifier pulses pass through a β-barium borate (BBO) crystal followed by a separation, independent focus, and time-syncing of the signal and idler pulses onto a 1 mm $AgGaS_2$ difference frequency crystal. The OPA produces mid-IR pulses tunable between 3 and 7 μm (3300−1400 cm^{-1}) with pulse durations of 95 fs at 5 μm and 1−2 μJ/pulse. The remainder of the amplifier pulse was frequency doubled by means of a 0.1 mm BBO crystal and compressed with a pair of fused silica prisms to a final pulse

† Part of the special issue "Robert J. Silbey Festschrift".

10.1021/jp0603738 CCC: $33.50
Published on Web 06/22/2006

duration of 80 fs and pulse energy reduced to 1 μJ/pulse by means of a $\lambda/2$ waveplate and polarizer placed prior to the doubling crystal. The 400 nm and mid-IR pulses were focused onto a 100 μm thick flowing or spinning sample cell with 2 mm calcium fluoride windows. The pulses were arranged in a parallel polarization configuration, and temporal overlap was found by replacing the back window of the sample cell with a ZnSe window, resulting in a large, long lived transient absorption signal. The signal was spectrally resolved using a Triax 180 imaging spectrometer (Jobin-Yvon Horiba) with grating appropriate to supply 4 cm^{-1} resolution. Detection of the mid-IR pulses was done with a 32-element HgCdTe array detector (Infrared Associates) attached to an IR32-16 multichannel laser pulse system (Infrared Systems Development Corp.). The detection was triggered by the fundamental laser repetition rate and an output frequency of a phase locked chopper inserted into the pump beam. One point to take into consideration in our experiments is that while in electronic spectroscopy one is able to directly correlate signal intensity with electronic state population, when using the mid-IR as the probe wavelength signal intensity can also arise from the changes in dipole strength by time-dependent electron density modulations.

Steady state absorption spectra were measured using a Shimadzu UV-1601 spectrometer. Steady state fluorescence data were collected using a Spex Fluorolog-τ2 with a red extended Hamamatsu photomultiplier tube (model no. R2659). The concentrations used for the transient absorption experiments were low (typically 1 mg/mL, $\sim 1 \times 10^{-4}$ M), so as to avoid the formation of bicimers.[27,32] The presence of cis isomers, which we want to avoid, is also concentration dependent.[38] The steady state absorption spectra were collected with sample concentrations so as to produce a maximum absorption of $\sim$0.5. The steady state fluorescence spectra were obtained by diluting the samples used for absorption by a factor of 10.

Time resolved fluorescence measurements were performed using a time correlated single photon counting (TCSPC) apparatus set at the magic angle polarization. A Coherent Inc. mode locked femtosecond laser (Mira 900) with a diode pumped, frequency doubled Nd:YVO_4 (Verdi V-10, Coherent) was used as the excitation source. The output beam was frequency doubled using a 1.5 mm thick BBO crystal. The repetition rate was reduced from 76 to 3.8 MHz using an extra cavity pulse picker, giving a center wavelength of 400 nm and a pulse energy of $\sim$3 nJ. Emission was selected using a double grating monochromator (DH10 VIR, Jobin Yvon) with a spectral band-pass of 4 nm at the emission maximum in a 1 cm path length stirred sample cell. The signal was collected by means of a multichannel plate (Hamamatsu MCP model no. R28094-01) and a single photon counting card (Boston Electronics SPC-630) set for 5.5 ps/channel. All standard solvents were used as received from Sigma Aldrich and were of the best spectroscopic grade available. Deuterated solvents were used as obtained from Cambridge Isotope Labs. DCM was obtained from Exciton without further purification. High performance liquid chromatography of fresh samples of DCM solution exhibit only one elutant peak, which is attributed to the trans form of DCM.[18,38] Upon equilibration in room light for 24 h, the elutant peak from the trans form splits into two distinct visible absorptions and the newly arising peak is assigned to the cis form of DCM which has slightly stronger absorption to the blue side of the trans absorption. Transient absorption experiments performed using either fresh or light equilibrated samples show no difference in lifetimes, intensities, or dynamics of the vibrational bands observed.

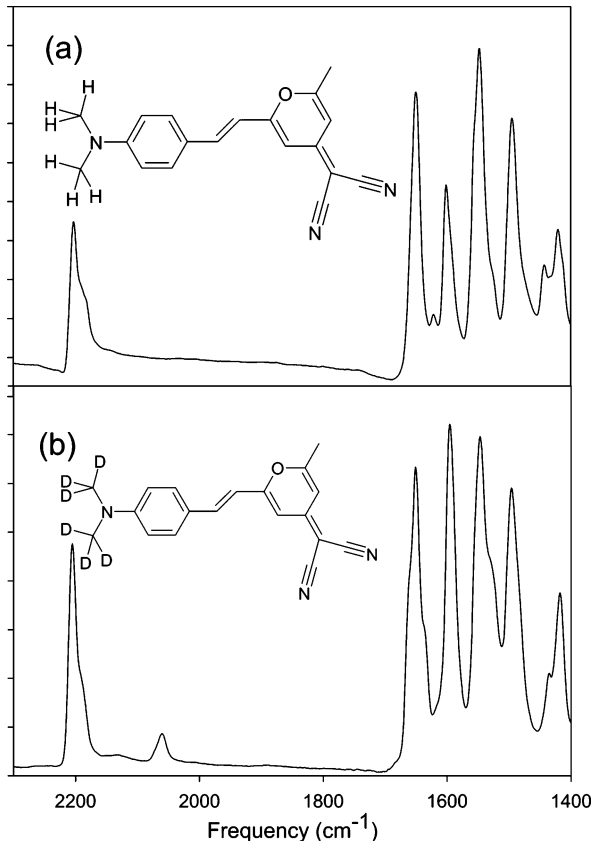

Figure 1. Infrared spectra of DCM (a) and its isotopomer DCM-d_6 (b). The structures of both molecules are shown above their respective spectra.

Visualization of the vibrational modes is made possible by calculating the vibrational spectrum with density functional theory (DFT) using the BLYP 6-31G(d) basis set in the QChem package,[39] extracting the vibrational normal modes, and viewing them using the Molekel molecular graphics package.[40]

Synthesis of DCM-d_6

The synthesis of DCM-d_6 primarily followed a previously reported synthesis;[41] a short summary follows. (2,6-Dimethyl-4*H*-pyran-4-ylidene)-malononitrile was synthesized by refluxing 2,6-dimethyl-γ-pyrone and malononitrile in the presence of acetic anhydride for 45 min followed by removal of the resultant acetic acid under vacuum and recrystallization from cyclohexane.[42] Dimethylaniline-d_6 was synthesized from freshly distilled aniline and iodomethane-d_3 in the presence of sodium carbonate.[43] To form the aldehyde, dimethylaniline-d_6 underwent a Vilsmeir formylation with pyrophosphoryl chloride and dimethyl formamide and was sublimed in a Kugelrohr apparatus to give 4-dimethylaminobenzaldehyde-d_6.[44] DCM-d_6 was formed by the reaction of 4-dimethylaminobenzaldehyde-d_6 and (2,6-dimethyl-4*H*-pyran-4-ylidene)malononitrile in the presence of piperidine. The final purification was done without recrystallization, and the retention factor of DCM was found to be 0.9 for chloroform on Whatman PK6F TLC plates, by cospotting with the commercial DCM, contrary to the retention factor of 0.1 that was reported in ref 41.

Results

The effect of the deuterium substitution on the ground state infrared absorption frequencies along with the structures of both isotopomers are depicted in Figure 1. The Fourier transform

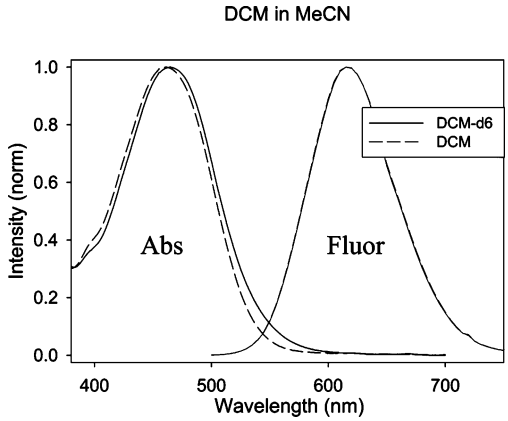

Figure 2. Absorption and fluorescence spectra of DCM (solid line) and DCM-d_6 (dashed line) in MeCN-d_3. DCM-d_6 absorption is red shifted 178 cm^{-1} from DCM, while the fluorescence spectra are indistinguishable.

infrared (FTIR) spectra shown in Figure 1 illustrate the presence of a new absorption band at ~2050 cm^{-1} in DCM-d_6 which is red shifted from ~3000 cm^{-1} in DCM due to the change in reduced mass of the C−D bond.

A summary of all steady state measurements is presented in Table 1 for the solvents dimethyl sulfoxide (DMSO) and acetonitrile (MeCN). As shown in the table, the visible absorption spectrum of DCM undergoes a slight red shift upon deuteration (~175−250 cm^{-1}), but the center frequency of the fluorescence spectrum remains unchanged between DCM and DCM-d_6. This shift in absorption can simply be attributed to a change in the zero point energy upon deuterium substitution and the difference between the anharmonicities of the ground and locally excited (LE) state. The fluorescence quantum yield of DCM-d_6, however, is decreased quite substantially, by 24%

TABLE 1: Steady State Spectral Data for DCM and DCM-d_6[a]

solvent		abs max (nm)	abs diff (cm^{-1})	fluor max (nm)	τ_{av} (ns)	Φ(d6)/Φ(h6)
DMSO	DCM	479.5	258	634	2.13	0.76
	DCM-d_6	485.5		634	2.40	
CH_3CN	DCM	460.4	178	615	1.65	0.83
	DCM-d_6	464.2		615	1.80	

[a] abs diff, difference in absorption maxima between isotopomers; τ_{av}, average fluorescence lifetime determined via eq 1; Φ(d6)/Φ(h6): ratio of fluorescence quantum yields for the isotopomers.

in DMSO and 17% in acetonitrile compared to DCM. Figure 2 shows that the steady state absorption spectra for both DCM and DCM-d_6 in MeCN have similar line shapes. The fluorescence spectra for both molecules however remain unaffected in both solvents we studied. The average fluorescence lifetimes (τ_{av}) listed in Table 1 were determined from eq 1:

$$\langle\tau\rangle = \frac{a_1}{a_1 + a_2}\tau_1 + \frac{a_2}{a_1 + a_2}\tau_2 \qquad (1)$$

where a is the amplitude of the exponential component and τ is the lifetime. This equation was applied to the results of fits to the TCSPC traces which contained three time scales: a rapid rise, with a time scale of approximately one-quarter of the instrument response of our apparatus, and two decay components. The rise times were excluded from the calculation of the average fluorescence lifetime, since the lifetime of this component is so short that the values of τ_{av} calculated using this rise were altered by no more than ~1%.

The mid-IR (shown from 1440 to 1620 cm^{-1}) transient absorption contour plots presented in Figure 3 were collected by calculating the change in optical density (ΔOD) induced by

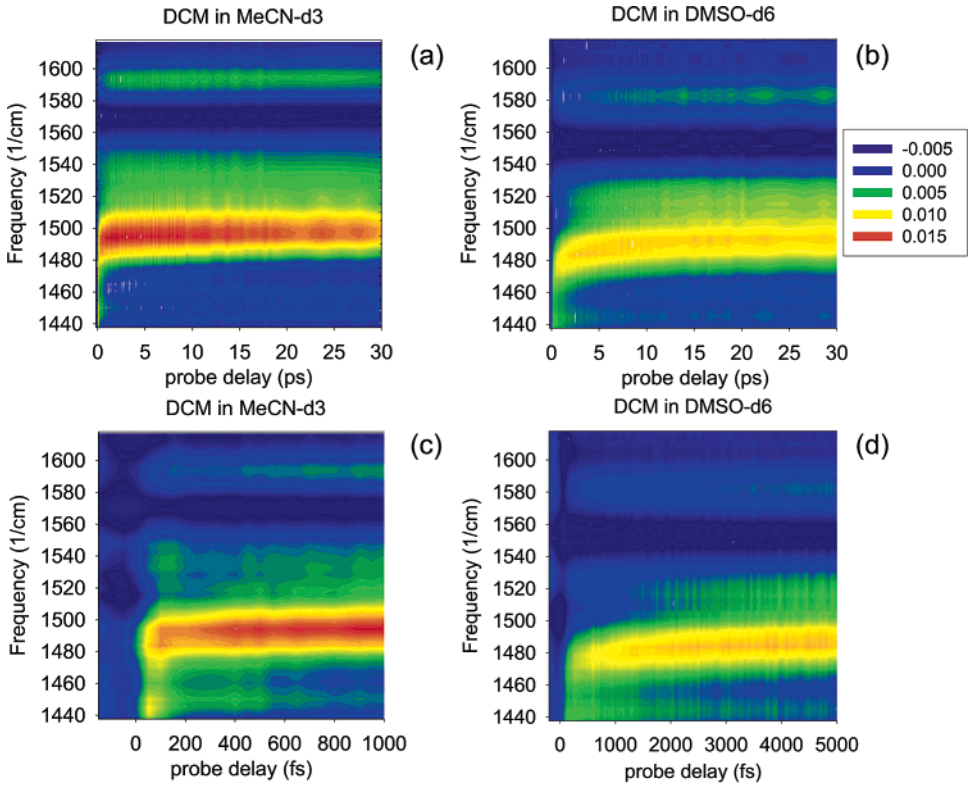

Figure 3. Transient infrared absorption contour plots of frequency vs probe delay for DCM in (a) MeCN-d_3 and (b) DMSO-d_6. Plots c and d show the same data as parts a and b, respectively, but on shorter time scales to show the fast shifting of the 1495 cm^{-1} band. Note that the time axes of panels c and d differ.

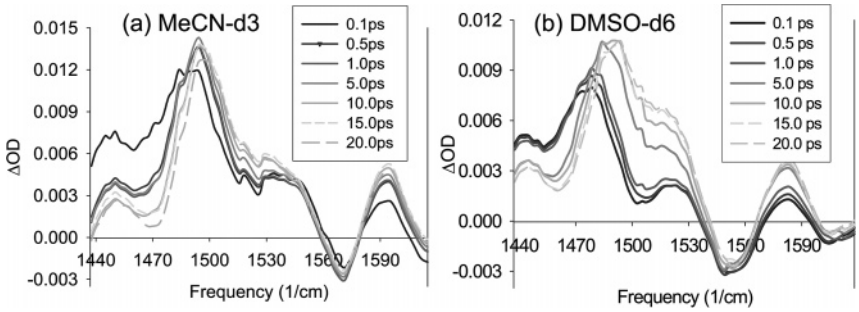

Figure 4. ΔOD vs frequency slices through the surfaces in Figure 3 at multiple probe delays for DCM in (a) MeCN-d_3 and (b) DMSO-d_6.

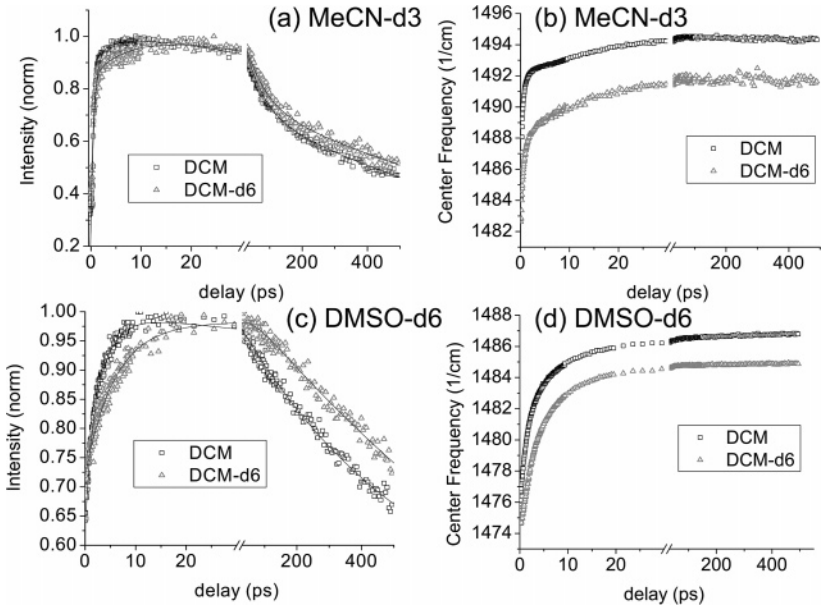

Figure 5. Decay of the maximum of the ∼1495 cm^{-1} peak shown for DCM in (a) MeCN-d_3 and (c) DMSO-d_6. The center frequency of the ∼1495 cm^{-1} peak is shown in part b for MeCN-d_3 and in part d for DMSO-d_6. Note the break in the time axes.

400 nm excitation of DCM using an average of 200 pulses per delay time and taking at least 10 scans over the entire delay time scale, up to a maximum of 500 ps. Deuterated solvents were chosen so as to avoid overlap with the solute peaks of interest by shifting the solvent absorptions to lower frequencies. The spectra in acetonitrile and DMSO contain several distinct absorption features: a peak at ∼1440 cm^{-1} that has an instrument-response-limited rise and undergoes almost solely relaxation (decay) dynamics and a higher frequency peak (∼1495 cm^{-1}) that undergoes a blue shift of its center frequency as well as more complex intensity changes. The other absorptions in these spectra are at 1520 and 1590 cm^{-1} whose center frequencies do not shift but undergo changes on the same time scales as those of the 1495 cm^{-1} band. Fits of the intensity dependence of the 1495, 1520, and 1590 cm^{-1} peaks require multiple exponential components, with both positive and negative amplitudes. The band at 1440 cm^{-1} with its instrument-response-limited rise is assigned to the LE state of DCM, while the higher frequency absorptions (1495, 1520, and 1590 cm^{-1}) are assigned to the CT state. The plots in Figures 3 and 4 also show a slight solvent dependence of the center frequency of the absorption bands. The terminal frequencies of all the excited state bands scale linearly with the Ooshika−Lippert−Mattaga solvent polarity function[13−16] which is a function of the dielectric constant and index of refraction of the solvent; the slopes of these fits are 1.5 times greater for the CT bands than for the LE band. This strong solvent influence on the CT bands is most likely due to the increase in dipole moment in the CT state.

Figure 4 shows frequency slices of all features in the fingerprint region (from 1440 to 1620 cm^{-1}) to emphasize the dynamics, specifically the fast initial decay of the LE band (∼1−2 ps) and the sharp rise (and frequency shift for the 1495 cm^{-1} band) in the CT absorption bands. We attribute the fast rise in the CT bands to the rapid evolution of the LE state into the CT state. No excited state features were observed between the region shown and the CN stretch at 2208 cm^{-1}.

These spectra were fit by a sum of Gaussians to more accurately separate the contributions to the peak intensity from line width changes and center frequency shifting from rise and decay. The kinetic traces shown in Figure 5 are constructed from these Gaussian fits. Parts a and c of Figure 5 show the Gaussian normalized amplitude of the ∼1495 cm^{-1} feature for MeCN-d_3 and DMSO-d_6 solvents, respectively, while parts b and d show the center frequency of this band versus probe delay times in the same solvents. The center frequencies of the 1520 and 1590 cm^{-1} bands were not affected by the methyl deuteration. The plots of the intensity of the 1495 cm^{-1} band versus time in Figure 5a and c both show a fast rise (∼1−3 ps), a midrange growth (∼10−30 ps), especially notable in DMSO-d_6, and long time (>500 ps) decay of the absorption in both DCM and DCM-d_6. It is interesting to note that the shifting time scale of the band is also markedly faster in DCM than in DCM-d_6; this is the most apparent in the case of MeCN-d_3 solution due to the extremely short solvation time scales, as shown in Figure 5b and d, showing that both molecular structure and solvation play a role in determining the time scale of CT

TABLE 2: 1495 cm^{-1} Band Dynamics and Solvation Time Scales[a]

DMSO-d_6				
			solvation time[b]	
shift	a_i (cm^{-1})	τ_i (ps)	a_i	τ_i (ps)
DCM	6.6	1.6	0.5	0.21
	4.5	10	0.41	2.3
	$\langle t \rangle$	5.0 ± 2.1	0.092	11
DCM-d_6	8.2	3.4	$\langle t \rangle$	2.0
	2.7	14		
	$\langle t \rangle$	6.0 ± 2.4		

decay	a_i	τ_i (ps)
DCM	−0.31	2.6
	−0.062	34
	$\langle t \rangle$ rise	7.8 ± 0.9
	0.14	120
	0.90	1730
	$\langle t \rangle$ decay	1500 ± 300
DCM-d_6	−0.25	6.6
	−0.066	40
	$\langle t \rangle$ rise	13.5 ± 1.5
	0.046	100
	1.0	1750
	$\langle t \rangle$ decay	1700 ± 1100

MeCN-d_3				
			solvation time[b]	
shift	a_i (cm^{-1})	τ_i (ps)	a_i	τ_i (ps)
DCM	9.5	0.34	0.69	0.089
	2.6	13	0.31	0.63
	$\langle t \rangle$	3.1 ± 1.5	$\langle t \rangle$	0.26
DCM-d_6	6.0	0.57		
	3.9	12		
	$\langle t \rangle$	5.1 ± 2.5		

decay	a_i	τ_i (ps)
DCM	−0.67	0.54
	−0.19	7.9
	$\langle t \rangle$ rise	2.20 ± 0.17
	0.39	59
	0.91	1130
	$\langle t \rangle$ decay	810 ± 190
DCM-d_6	−0.85	0.47
	−0.27	11
	$\langle t \rangle$ rise	3.5 ± 1.1
	0.36	59
	0.76	1250
	$\langle t \rangle$ decay	900 ± 500

[a] a_i, amplitude of the exponential component; τ_i, lifetime of the exponential component; $\langle \tau \rangle$, average lifetime determined via eq 1. [b] The time scales of solvation for DMSO and MeCN are taken from Maroncelli and co-workers.[48]

formation. Table 2 collects the parameters obtained from fits of the data presented in Figure 5 for both the shifting of the center frequency and population dynamics as well as solvation time scales for both solvents measured by Maroncelli and co-workers using coumarin 153 as the probe.[48]

Figure 6 shows kinetic traces in DMSO-d_6 (a) for the CN triple bond symmetric stretch ground state bleach dynamics at 2208 cm^{-1} and (b) the excited state dynamics at 2182 cm^{-1} for both DCM and DCM-d_6 (scaled for comparison). There is a second excited state absorption band at 2158 cm^{-1} which has identical kinetics to the 2182 cm^{-1} band shown in Figure 6b, as it arises from the accompanying asymmetric stretch of the dicyano group, but the analogous stretch in the ground state does not appear in the spectra because it is masked by the large cross section of the ground state symmetric stretch. The kinetics for DCM and DCM-d_6 are very similar for these frequencies, with the excited state absorption band showing a sharp spike arising from the solvent (and present in pure solvent), followed by a very slow decay (∼10% in 500 ps).

Discussion

The time resolved infrared spectra of DCM in polar solvents clearly show that the excited state electronic structure evolves in a solvent-dependent manner from that created directly by optical excitation. The instrument-limited change in the CN triple bond symmetric stretch frequency suggests charge separation and localization on the cyanomethylene acceptor groups occurs immediately upon excitation. The fact that no further changes in the CN stretch frequency are observed suggests that the RICT state, like that proposed for DMABN,[4] in which the cyano carbon becomes sp^2 hybridized is not accessible for DCM.

We have no direct evidence to suggest that the S_1 LE state is the one populated by optical excitation rather than via radiationless relaxation from S_2, as appears to be the case for DMABN.[36] However, the solvent-dependent evolution of the IR spectra do imply that if S_1 is populated via S_2 motion through the conical intersection, this does not lead to a wide range of torsional angles for the dimethyl amino group being populated at very short times, since this would lead to a broad range of frequencies for the 1495 cm^{-1} region.

The short time evolution we see involves the dimethyl amino group most likely rotating out of place (and pyramidalizing[4,46]), giving rise to a deuterium- and solvent-dependent frequency shift of the 1495 cm^{-1} band. Since the center frequencies of the 1520 and 1590 cm^{-1} bands do not shift, their modes must be independent of the torsional angle of the dimethylamino group within our model. Yoshizawa et al., using a stimulated Raman method in DMSO solution, report vibrational bands at 1470 and 2150 cm^{-1} which they assign to a state intermediate between trans and cis.[47] However, their time and spectral resolutions of 250 fs and 25 cm^{-1}, respectively, are inadequate to reveal the short time dynamics shown in Figures 3−5.

The identity of the 1495 cm^{-1} band is not trivial to establish unambiguously. Figure 7 shows the displacement vectors for the calculated mode in the ground state of DCM that serves as the most likely candidate from our calculations. It involves considerable motion of the carbon skeleton of the molecule and has no contribution from the CN groups. In Table 2, we compare the time scales of the shift in frequency of the 1495 cm^{-1} band for DCM and DCM-d_6 with solvation times for DMSO-d_6 and MeCN-d_3 obtained from Stokes shift measurements by Maroncelli and co-workers.[45,48] We find a very fast component in the shift for acetonitrile solution, consistent with the amplitude of ∼100 fs relaxation in the solvation response in acetonitrile, while for DMSO we do not observe an ultrafast component in the shift, although an ∼200 fs component is present in the solvation reponse. The average shifting time ($\langle \tau \rangle$), presented in Table 2, is determined using eq 1. The average shifting time is shorter in acetonitrile than DMSO (3.1 ps vs 5.0 ps), and in each case, $\langle \tau \rangle$ is smaller for DCM than for DCM-d_6. The comparison of solvation time scales with the shift time scales is complex for several reasons: First, the frequency change results from motion on the excited state potential surface, and its time scale will be set by the shape of the surface as well as the solvent time scales. In addition, the strength of the IR transition may change during the relaxation, and it may change differently for DCM and DCM-d_6, since the nature of the mode (and its couplings to other modes) is different in the two molecules. Table 2 shows that the average shift times and rise times for the intensity of

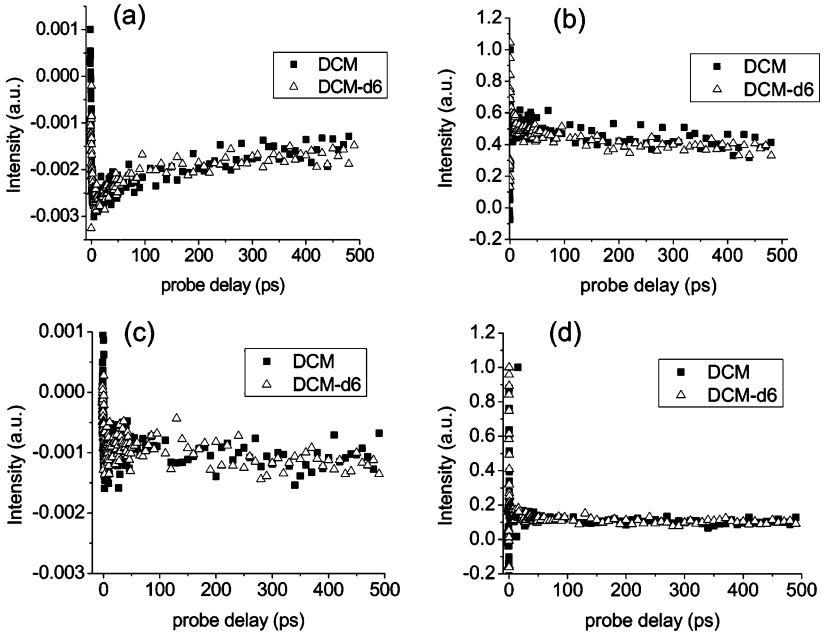

Figure 6. (a and c) Intensity vs probe delay at 2208 cm^{-1} (ground state CN stretch) of DCM and DCM-d_6 in DMSO-d_6 (a) and MeCN-d_3 (c). (b and d) Intensity vs probe delay at 2182 cm^{-1} (excited state CN stretch) in DMSO-d_6 (b) and MeCN-d_3 (d).

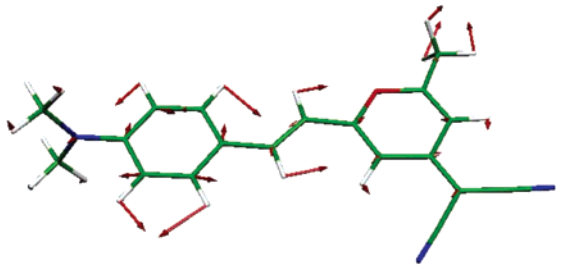

Figure 7. Calculated dispacement vectors in the ground state of DCM for the mode that we suggest to give rise to the 1495 cm^{-1} band (see Materials and Methods).

the mode are, however, quite similar and show the same trends with deuteration and change of solvent, suggesting these times can, at least roughly, be associated with population changes. We therefore associate time scales of 5−8 ps (DMSO-d_6) and 2−3 ps (MeCN-d_3) with formation of the TICT state in DCM. Similarly, time scales of 6−14 ps and 3−5 ps correspond to TICT formation in DCM-d_6 in DMSO-d_6 and MeCN-d_3, respectively. Following the calculations of Gomez et al.,[36] we expect the TICT state to involve both twisting and pyramidalization of the C−N(Me_2) group. The average decay times for the CT modes are quite similar for DCM and DCM-d_6 in each solution (with the d_6 molecule having slightly slower decays in both solvents) but vary by a factor of 2 from DMSO-d_6 to MeCN-d_3. The average fluorescence lifetimes (Table 1) are longer than the vibrational "lifetimes" listed in Table 2, and the difference between DMSO-d_6 and MeCN-d_3 solutions is much smaller (14% vs 47%). Clearly, this hints at more complex excited state behavior than simple LE-TICT equilibration and subsequent decay on an ∼2 ns time scale, but equilibration and intramolecular vibrational relaxation within the TICT minimum presumably lead to configurations with a much weaker oscillator strength for the 1495 cm^{-1} mode.

If the observed spectral dynamics involves rapid LE-to-CT conversion, we must also consider the role of excess vibrational energy on the spectra, following the transition. Previous studies of 2-(2′-hydroxyphenyl)benzothiazole[6] and *trans*-stilbene[49] have found similar blue shifts in all the bands of their vibrational spectra as a result of vibrational relaxation. The time scales of these shifts were compared in solvents of varying thermal diffusivity, and as might be expected, the relaxation rate increased with increasing thermal diffusivity. While this general trend holds for the 1495 cm^{-1} mode, if the average lifetimes are compared, the amplitudes of the shift are much larger than those found in stilbene and benzothiazole, the lifetimes of which are much shorter (by nearly an order of magnitude in the case of the longest time scales). In addition, only a single band shows the upshifting while all other observed bands have only amplitude changes. Also, we do not expect a significant amount of vibrational energy to be released in the LE-to-CT transition, since the process occurs on a time scale of a few picoseconds. We therefore conclude that vibrational relaxation can be ruled out as the cause of the shift we observe. If the shift was a manifestation of vibrational cooling, we would expect to also observe shifts in the 1440, 1520, 1590, and 2182 cm^{-1} bands, which is not the case.

The fluorescence quantum yield is significantly lower in DCM-d_6 than in DCM (Table 1), even though the average fluorescence lifetime is very similar in both isotopomers. This means that the radiative rate decreases by almost the same amount that the nonradiative rate increases in DCM-d_6. A change of ∼10% in each is consistent with the measurements. In a conventional relaxation process, the excited state energy is converted into C−H stretch energy and subsequently transferred into the local solvent modes. One would normally expect that the deuterium substitution would increase the lifetime because it would slow the internal conversion, in contrast to our observation.

Up to this point, we have not discussed the second pathway of excited state decay, trans to cis isomerization. The quantum yield of this process has measured for both DMSO and MeCN solutions as 0.014 and 0.011, respectively.[18,20] With such a small yield, it seems unlikely that the strong IR bands described result from this process.

Conclusion

In this study, we have presented mid-IR transient absorption experiments on DCM and its deuterated isotopomer DCM-d_6 in two solvents of differing polarities and solvation time scales.

Our goal in this experiment was to gain insight into the structural dynamics of the CT species responsible for the long lived fluorescence. Our data on the CN excited and ground state stretches clearly show that the CT state does not involve twisting or some other molecular reshaping occurring at the cyanomethylene end of the molecule. We attribute the striking shift in frequency and change in amplitude of the 1495 cm^{-1} mode that occur after the formation of the excited state to formation of the charge transfer state via twisting and pyramidalization of the $C-N(Me)_2$ group, and concomitant changes in C−C bonding character throughout the molecule. The remarkable insensitivity of the frequencies of the CN modes and the 1440, 1520, and 1590 cm^{-1} modes after excitation along with the solvent-dependent time scales for the shift and amplitude changes in the 1495 cm^{-1} model lead us to rule out vibrational relaxation as the origin of the observed effects. A more quantitative analysis requires much more detailed confrontation of theory and experiment. We hope that the type of sophisticated calculation described by Robb and co-workers for DMABN[36] can be extended, via trajectory studies, to explore the evolution of the vibrational spectra of prototypical molecules exemplifying the complex electronic and structural dynamics exhibited by DCM and DMABN, for example. Such a comparison should enable much closer connection of theory and experiment in the area of conical intersection-mediated excited state dynamics, an area that is revolutionizing the understanding of organic photochemistry.[50]

Acknowledgment. This work was supported by the NSF. We thank Justin Mynar and Jean M. J. Fréchet for their generous donation of lab space and assistance with the synthesis of the DCM-d_6 compound.

References and Notes

(1) Herbst, J.; Heyne, K.; Diller, R. *Science* **2002**, *297*, 822.
(2) Chudoba, C.; Kummrow, A.; Dreyer, J.; Stenger, J.; Nibbering, E. T. J.; Elsaesser, T.; Zachariasse, K. A. *Chem. Phys. Lett.* **1999**, *309*, 357.
(3) Chudoba, C.; Nibbering, E. T. J.; Elsaesser, T. *Phys. Rev. Lett.* **1998**, *81*, 3010.
(4) Dreyer, J.; Kummrow, A. *J. Am. Chem. Soc.* **2000**, *122*, 2577.
(5) Ma, C.; Kwok, W. M.; Matousek, P.; Parker, A. W.; Phillips, D.; Toner, W. T.; Towrie, M. *J. Raman Spectrosc.* **2001**, *32*, 115.
(6) Rini, M.; Dreyer, J.; Nibbering, E. T. J.; Elsaesser, T. *Chem. Phys. Lett.* **2003**, *374*, 13.
(7) Nibbering, E. T. J.; Fidder, H.; Pines, E. *Annu. Rev. Phys. Chem.* **2005**, *56*, 337.
(8) Liu, Z. G.; Chen, Z. J.; Gong, Q. H. *Chin. Phys. Lett.* **2005**, *22*, 1536.
(9) Wang, B. C.; Liao, H. R.; Chen, W. H.; Chou, Y. M.; Yeh, J. T.; Chang, J. C. *THEOCHEM* **2005**, *716*, 19.
(10) Berner, D.; Houili, H.; Leo, W.; Zuppiroli, L. *Phys. Status Solidi A* **2005**, *202*, 9.
(11) Mori, T.; Kim, H. G.; Mizutani, T.; Lee, D. C. *Jpn. J. Appl. Phys., Part 1* **2001**, *40*, 5346.
(12) Cheon, C. H.; Joo, S. H.; Kim, K.; Jin, J. I.; Shin, H. W.; Kim, Y. R. *Macromolecules* **2005**, *38*, 6336.
(13) Meyer, M.; Mialoco, J. C. *Opt. Commun.* **1987**, *64*, 264.
(14) Ooshika, Y. *J. Phys. Soc. Jpn.* **1954**, *9*, 594.
(15) Mataga, N.; Kaifu, Y.; Koizumi, M. *Bull. Chem. Soc. Jpn.* **1956**, *29*, 465.
(16) Lippert, E. *Z. Naturforsch., A: Phys. Sci.* **1955**, *10*, 541.
(17) Meyer, M.; Mialocq, J. C.; Rougee, M. *Chem. Phys. Lett.* **1988**, *150*, 484.
(18) Meyer, M.; Mialocq, J. C.; Perly, B. *J. Phys. Chem.* **1990**, *94*, 98.
(19) Marguet, S.; Mialocq, J. C.; Millie, P.; Berthier, G.; Momicchioli, F. *Chem. Phys.* **1992**, *160*, 265.
(20) Mialocq, J. C.; Armand, X.; Marguet, S. *J. Photochem. Photobiol., A* **1993**, *69*, 351.
(21) Martin, M. M.; Plaza, P.; Meyer, Y. H. *Chem. Phys.* **1995**, *192*, 367.
(22) Gustavsson, T.; Baldacchino, G.; Mialocq, J.-C.; Pommeret, S. *Chem. Phys. Lett.* **1995**, *236*, 587.
(23) Pommeret, S.; Gustavsson, T.; Naskrecki, R.; Baldacchino, G.; Mialocq, J. C. *J. Mol. Liq.* **1995**, *64*, 101.
(24) Zhang, H.; Jonkman, A. M.; Vandermeulen, P.; Glasbeek, M. *Chem. Phys. Lett.* **1994**, *224*, 551.
(25) Dahl, K.; Biswas, R.; Ito, N.; Maroncelli, M. *J. Phys. Chem. B* **2005**, *109*, 1563.
(26) Abraham, E.; Oberlé, J.; Jonusauskas, G.; Lapouyade, R.; Rullière, C. *Chem. Phys.* **1997**, *214*, 409.
(27) Gilabert, E.; Lapouyade, R.; Rullière, C. *Chem. Phys. Lett.* **1991**, *82*, 82.
(28) Hashimoto, M.; Hamaguchi, H.-O. *J. Phys. Chem.* **1995**, *99*, 7875.
(29) Kwok, W. M.; Ma, C.; Matousek, P.; Parker, A. W.; Phillips, D.; Toner, W. T.; Towrie, M.; Umapathy, S. *J. Phys. Chem. A* **2001**, *105*, 984.
(30) Lapouyade, R.; Kuhn, A.; Letard, J.-F.; Rettig, W. *Chem. Phys. Lett.* **1993**, *208*, 48.
(31) Rettig, W.; Majenz, W. *Chem. Phys. Lett.* **1989**, *154*, 335.
(32) Viallet, J.-M.; Dupuy, F.; Lapouyade, R.; Rulliere, C. *Chem. Phys. Lett.* **1994**, *222*, 571.
(33) Oberlé, J.; Abraham, E.; Jonusauskas, G.; Rullière, C. *J. Raman Spectrosc.* **2000**, *31*, 311.
(34) Rettig, W.; Majenz, W. *Chem. Phys. Lett.* **1989**, *154*, 335.
(35) Abraham, E.; Oberlé, J.; Jonusauskas, G.; Lapouyade, R.; Rullière, C. *J. Photochem. Photobiol., A* **1997**, *105*, 101.
(36) Gomez, I.; Reguero, M.; Boggio-Pasqua, M.; Robb, M. A. *J. Am. Chem. Soc.* **2005**, *127*, 7119.
(37) Hamm, P.; Kaindl, R. A.; Stenger, J. *Opt. Lett.* **2000**, *25*, 1798.
(38) Drake, J. M.; Lesiecki, M. L.; Camaioni, D. M. *Chem. Phys. Lett.* **1985**, *113*, 530.
(39) Kong, J.; White, C. A.; Krylov, A. I.; Sherrill, D.; Adamson, R. D.; Furlani, T. R.; Lee, M. S.; Lee, A. M.; Gwaltney, S. R.; Adams, T. R.; Ochsenfeld, C.; Gilbert, A. T. B.; Kedziora, G. S.; Rassolov, V. A.; Maurice, D. R.; Nair, N.; Shao, Y. H.; Besley, N. A.; Maslen, P. E.; Dombroski, J. P.; Daschel, H.; Zhang, W. M.; Korambath, P. P.; Baker, J.; Byrd, E. F. C.; Van Voorhis, T.; Oumi, M.; Hirata, S.; Hsu, C. P.; Ishikawa, N.; Florian, J.; Warshel, A.; Johnson, B. G.; Gill, P. M. W.; Head-Gordon, M.; Pople, J. A. *J. Comput. Chem.* **2000**, *21*, 1532.
(40) Flükiger, P.; Lüthi, H. P.; Portmann, S.; Weber, J. *MOLEKEL 4.3*; Swiss Center for Scientific Computing: Manno, Switzerland, 2000−2002.
(41) Bourson, J.; Valeur, B. *J. Phys. Chem.* **1989**, *93*, 3871.
(42) Woods, L. L. *J. Am. Chem. Soc.* **1958**, *80*, 1440.
(43) Bertrand, S.; Hoffmann, N.; Humbel, S.; Pete, J. P. *J. Org. Chem.* **2000**, *65*, 8690.
(44) Downie, I. M.; Earle, M. J.; Heaney, H.; Shuhaibar, K. F. *Tetrahedron* **1993**, *49*, 4015.
(45) Maroncelli, M.; Fleming, G. R. *J. Chem. Phys.* **1987**, *86*, 6221.
(46) Rettig, W.; Zietz, B. *Chem. Phys. Lett.* **2000**, *317*, 187.
(47) Yoshizawa, M.; Kubo, M.; Kurosawa, M. *J. Lumin.* **2000**, *87−9*, 739.
(48) Horng, M. L.; Gardecki, J. A.; Papazyan, A.; Maroncelli, M. *J. Phys. Chem.* **1995**, *99*, 17311.
(49) Iwata, K.; Hamaguchi, H. *J. Phys. Chem. A* **1997**, *101*, 632.
(50) Migani, A., Olivucci, M. Conical Intersections and Organic Reaction Mechanisms. In *Conical Intersections: Electronic Structure, Dynamics and Spectroscopy*; Domcke, W., Yarkony, D. R., Köppel, H., Ed.; World Scientific: London, 2004; Vol. 15; p 271.